J Comput Electron (2010) 9: 211–217
DOI 10.1007/s10825-010-0325-8

A semiclassical transport model for quantum cascade lasers based on the Pauli master equation

G. Milovanovic · H. Kosina

Published online: 15 October 2010

Abstract A semiclassical transport description based on the Pauli master equation (PME) is presented. A Monte Carlo simulator has been developed, which is an efficient approach for solving the PME and includes the most relevant scattering mechanisms. The proposed method has been used to simulate Quantum Cascade Lasers (QCLs) and allows the study of charge transport in an efficient way. As a prototypical example, we investigate a QCL in the THz region.

Keywords Pauli master equation · Monte Carlo · Quantum cascade laser · Semiclassical transport

1 Introduction

In 1970, Esaki and Tsu [1] proposed the usage of heterostructures for applications in optoelectronics. The first suggestion to use intersubband transitions in order to create a laser was made by Kazarinov and Suris [2]. Over the past several years, solid-state lasers based on intersubband transitions in semiconductor heterostructures have proved to be very promising candidates for practical sources of radiation [3]. Designed by means of band structure engineering, a successfully working QCL has first been reported in 1994 [4].

In the meantime, much theoretical and technological progress has been achieved in the development of QCLs which are unipolar devices made of a sequence of alternating wide band gap and narrow band gap semiconductor layers with typical thicknesses of a few nanometers. The multi quantum well structure is comprised of repeated stages of active regions sandwiched between electron injecting and collecting contacts. By applying a bias voltage, an electric current flows through the quantum cascade structure where electrons cascade down the quantized energy staircase.

Charge transport simulations according to the nonequilibrium Green's function (NEGF) method need enormous computation time for these structures and have to be carefully customized for each particular structure [5]. Theoretical studies showed that in many practical cases the steady state transport in QCLs is incoherent and the semiclassical description found to be satisfactory [6]. Although coherent oscillations of the population inversion were observed, the resulting steady state transport is incoherent as the oscillations are damped on the sub-picosecond timescale which is considerable shorter than the average transit time across one stage.

The PMEs can be solved by a Monte Carlo approach which allows one to include a large variety of scattering mechanisms on the microscopic level. The in-plane dynamics of the electrons is automatically taken into account. A big advantage of this simulation method is that it requires less computational time than the NEGF formalism.

However, the Monte Carlo approach is based on a semiclassical description and provides a well suited method for modeling transport in regimes where coherent transport plays a minor role [7].

The understanding of numerous physical processes is needed for the design and optimization of QCLs. Predominantly, suitable waveguiding and population inversion with appropriate radiative transitions are essential and must be provided by tailoring the band structure and scattering mechanisms. The Monte Carlo simulator developed is a reasonable analysis tool for these issues.

G. Milovanovic (✉) · H. Kosina
Institute for Microelectronics, TU Wien, Gußhausstraße 27–29/E360, 1040 Wien, Austria
e-mail: milovanovic@iue.tuwien.ac.at

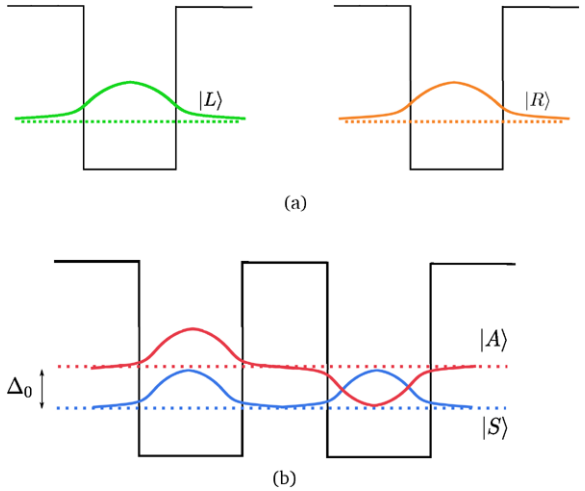

Fig. 1 Anitcrossing between two single well states

2 Theoretical framework

In the semiclassical model the transport is described via in- and out-scattering from stationary states that are solutions of the Schrödinger equation. Since the band edge formed by the wells and barriers is included in the Hamiltonian, tunneling is already considered through the eigenstates, and transport occurs via scattering between these states. Figure 1 illustrates how tunneling between two quantum well states $|L\rangle$ and $|R\rangle$ is described by solving the coupled well system and obtaining a new set of delocalized states. The anticrossing gap Δ_0 is the minimum separation between the symmetric and antisymmetric states.

Since the symmetric $|S\rangle$ and antisymmetric $|A\rangle$ states are solutions of the coupled well system, they are delocalized in the sense that they pass through both consecutive barrier and well layers. Using such delocalized states as basis functions, there is no interwell tunneling time, and intersubband scattering into and out of $|A\rangle$ and $|S\rangle$ from other subbands govern the transport through the barrier. It is shown that this picture is accurate for strong coupling, i.e. large Δ_0 [8].

When the electron dephasing length in the contacts $\lambda_\phi \sim \hbar v_{th}/\delta E_{th}$ is larger than the length of the device L, the electrons are considered to be "larger" than the device [9]. Here, v_{th} denotes the thermal velocity of the packet and δE_{th} the energetic broadening. In this case, the contacts inject only diagonal elements of the density matrix ρ.

Following Van Hove's observation, the time needed to build the off-diagonal elements of ρ is much longer than the relaxation and transit times [10]. Off-diagonal terms in ρ are built up long after the electron has gone through the device. Thus, a master equation considering only diagonal elements of the density matrix is sufficient to describe electron transport in devices of size $L < \lambda_\phi$ [9].

2.1 Transport equation

For one-dimensional, open systems, the equation describing transport and relaxation phenomena can be written as follows [11].

$$\frac{d}{dt} f_{\mathbf{k}\alpha} = \frac{d}{dt} f_{\mathbf{k}\alpha}\bigg|_{\text{scat}} + \frac{d}{dt} f_{\mathbf{k}\alpha}\bigg|_{\text{res}} \tag{1}$$

Here $\mathbf{k}$ is the in-plane wave vector and $\alpha \equiv (\lambda, \nu, \eta)$ denotes the generic electron state in the multi quantum well structure, i.e. λ is the stage, ν represents the subband index and η stands for the valley index.

Due to the smallness of the device and the assumption that the electrons are injected as delocalized objects, this approach is identical to the approach considered by Fischetti [12].

The first term on the r.h.s of (1) describes the scattering dynamics and is usually treated via collision operators. The master equation can be derived from the Liouville-von Neumann equation using a representation of eigenstates which diagonalize the external potential. The Markov approximation, which ensures the loss of memory effects [13], is the main assumption for the derivation. Fischetti uses additionally the Van Hove limit, which states that $\alpha_c^2 t$ is constant as $\alpha_c^2 \to 0$ and the time t tends to infinity, in order to derive the irreversible PME and to ensure that the off-diagonal terms of the density matrix remain negligible. α_c is the coupling constant of the Hamiltonian and determines the strength of the interaction, e.g. between electrons and phonons.

Iotti and coworkers present a somewhat different derivation of the same master equation, calling it Boltzmann-like equation [14]. They also start from the Liouville-von Neumann equation and apply the Markov approximation to the fully non-diagonal density matrix formulation. By introducing the diagonal approximation, the off-diagonal elements of the density matrix are neglected, and one arrives at the Boltzmann-like or PME.

$$\begin{aligned}\frac{d}{dt} f_{\mathbf{k}\alpha}(t)\bigg|_{\text{scat}} = \sum_{\mathbf{k}'\alpha'} \{ & S^{\alpha}_{\alpha'}(\mathbf{k}', \mathbf{k}) f_{\mathbf{k}'\alpha'}(t)[1 - f_{\mathbf{k}\alpha}(t)] \\ & - S^{\alpha'}_{\alpha}(\mathbf{k}, \mathbf{k}') f_{\mathbf{k}\alpha}(t)[1 - f_{\mathbf{k}'\alpha'}(t)]\}\end{aligned} \tag{2}$$

The transition rate $S^{\alpha'}_{\alpha}(\mathbf{k}, \mathbf{k}')$ from an initial state $|\mathbf{k}, \alpha\rangle$ to a final state $|\mathbf{k}', \alpha'\rangle$ can be calculated according to Fermis's Golden Rule [15]

$$S^{\alpha'}_{\alpha}(\mathbf{k}, \mathbf{k}') = \frac{2\pi}{\hbar} |\langle \mathbf{k}', \alpha' | H_{\text{int}} | \mathbf{k}, \alpha \rangle|^2 \delta(E(\mathbf{k}') - E(\mathbf{k}) \mp \hbar\omega) \tag{3}$$

where H_{int} denotes the interaction Hamiltonian. Basically, the semiclassical characterization is based on the assumption that the time between collisions, which is in the range of

sub-picoseconds, is large compared to the interaction time. The collisions are mutually independent and instantaneously change the electron momentum.

In general, (2) is suitable for studying steady state situations. Transient processes can not be described by the Pauli Master equation, since time dependent potentials are not weak perturbations according to the Van Hove treatment and the current continuity gets violated.

Due to the incoherent nature of the stationary charge transport in QCL heterostructures, the carrier distribution functions $f_{\mathbf{k}\alpha}$ are governed by the PME (2) [16]. Since no electric field is applied in the in-plane direction, (2) does not have the in-plane drift terms known from the Boltzmann equation. There is no diffusion term as well because of spatial uniformity in the interface plane. The electrons are not explicitly accelerated along the growth direction, rather the electronic states are affected through the change in the band profile which modifies the spatial electron distribution. Due to scattering the electrons are hopping among the subbands.

2.2 Boundary conditions

The second term on the r.h.s of (1) describes the open character of the system. It accounts for the injection and loss contributions from and to external carrier reservoirs and can be treated by a relaxation-time-like term of the following form.

$$\frac{d}{dt} f_{\mathbf{k}\alpha}\bigg|_{\text{res}} = \gamma_{\mathbf{k}\alpha}(f^0_{\mathbf{k}\alpha} - f_{\mathbf{k}\alpha}) \tag{4}$$

Here $\gamma^{-1}_{\mathbf{k}\alpha} = v_\perp |A_{\mathbf{k}\alpha}|^2$ is the device transit time of an electron, $v_\perp$ denotes the group velocity normal to the contact boundary and $A_{\mathbf{k}\alpha}$ is the amplitude of the incoming wave. $f^0_{\mathbf{k}\alpha}$ is assumed to be the quasi-equilibrium carrier distribution in the external reservoirs. This assumption is mainly based on the idea that the overall occupations of the "large" reservoirs of electrons are essentially unchanged by the addition or subtraction of a few electrons to or from the electronic states in the device [17].

In the course of solving the Schrödinger equation, a plane wave incident from outside the device is assumed which is partially reflected and transmitted. It is assumed that outside the device domain a plane wave is coming from $-\infty$ and is either transmitted to $+\infty$ or it is reflected by the potential and travels back to $-\infty$. The assumption that the wave function is continuous allows to specify the boundary conditions at the contacts. Introducing a reflexion coefficient R_α and transmission coefficient T_α, the total current flowing from the s-th contact into other contacts can be written as [12]

$$J^{(s)} = \sum_{\mathbf{k}\alpha}\left[\gamma^{(s)}_{\mathbf{k}\alpha}(f^{0,(s)}_{\mathbf{k}\alpha} - R^{(s)}_\alpha f^{(s)}_{\mathbf{k}\alpha}) - \sum_{r\neq s}\gamma^{(r)}_{\mathbf{k}\alpha} T^{(r)}_\alpha f^{(r)}_{\mathbf{k}\alpha}\right] \tag{5}$$

Since the QCL structure is translationally invariant, it is sufficient to simulate the electron transport over a generic central stage only. Due to the small wave function overlap between the central stage and the spatially remote stages, the interstage scattering can be assumed to be limited only to the nearest neighbor. The electron states corresponding to a single QCL stage are evaluated using a selfconsistent Schrödinger-Poisson solver. Given such carrier states, we consider the multi quantum well structure as a repetition of this periodicity region, which ensures the validity of charge conservation.

In this case, periodic boundary conditions can be imposed on the PME. The carrier transport is simulated over the central stage and every time a carrier proceeds an interstage scattering process, the electron is reinjected into the central region with an energy changed by $\Delta_{\lambda\lambda'} = eFL(\delta_{\lambda',\lambda+1} - \delta_{\lambda',\lambda-1})$ and the corresponding electron charge contributes to the current. F denotes the applied electric field and L is the length of the stage.

The current density across the device is given in terms of the net electron flux through the interface between the stages

$$J \propto \sum_{\mathbf{k}\nu\eta}\sum_{\mathbf{k}'\nu'\eta'}[S^{(\lambda+1)\nu'\eta'}_{\lambda\nu\eta}(\mathbf{k},\mathbf{k}')f_{\lambda\nu\eta}(\mathbf{k}) - S^{(\lambda-1)\nu'\eta'}_{\lambda\nu\eta}(\mathbf{k},\mathbf{k}')f_{\lambda\nu\eta}(\mathbf{k})] \tag{6}$$

In the Monte Carlo simulation, J is obtained by counting the interstage scattering events.

3 Physical models

From the infinite cascade we chose three stages as the domain for solving the Schrödinger equation

$$\left[-\frac{\hbar^2}{2}\frac{\partial}{\partial z}\frac{1}{\mathrm{m}^\star(z)}\frac{\partial}{\partial z} + \mathrm{V}_0(z) - eFz\right]\Psi_\alpha(z) = E_\alpha\Psi_\alpha(z) \tag{7}$$

selfconsistently with the Poisson equation, where E_α is the energy of state α, $\mathrm{m}^\star(z)$ denotes the effective mass, $\mathrm{V}_0(z)$ is the conduction band offset. We chose Dirichlet boundary conditions at the artificial boundaries, $\Psi_\alpha(0) = \Psi_\alpha(3L) = 0$.

The Fermi-Dirac distribution is used for the in-plane electron distribution in each subband. The obtained electron states are utilized to compute the scattering rates. The material dependent parameters appearing in the scattering rates can be looked up in Table 1.

3.1 Electron-LO phonon scattering

Usually, the scattering of electrons with LO phonons in a multi quantum well system is described by the Fröhlich interaction [18]. The scattering rate for an electron initially in

Table 1 Overview of the material parameters used in the simulation presented in this work, illustrated for the well and barrier material, respectively

	GaAs	$Al_{0.15}Ga_{0.85}As$
$m^\star_\Gamma$	0.067	0.075
$m^\star_X$	0.32	0.311
ϵ_S	12.90	12.47
ϵ_∞	10.89	10.48
χ_e [eV]	4.07	3.905
$\hbar\omega_{LO}$ [meV]	36.25	35.30
ρ [g/cm^3]	5.36	5.12
E_{ac} [eV]	3.6	3.49
E_{op} [eV]	5.9	6.0
$D_{\Gamma X}$ [eV/Å]	4.1	5.2

subband ν and stage λ to a final subband ν' and stage λ', is given by

$$\frac{1}{\tau^{\nu'\lambda'}_{\nu\lambda}(\mathbf{k}_\parallel)} = \frac{e^2\hbar\omega_{LO}m^\star_{\nu'\lambda'}}{4\hbar^3}\left(\frac{1}{\varepsilon_\infty}-\frac{1}{\varepsilon_S}\right)\left(N_{LO}+\frac{1}{2}\mp\frac{1}{2}\right) \times \int dq_z \frac{|\mathrm{F}^{\nu\lambda}_{\nu'\lambda'}(q_z)|^2}{q_z^4+(Q^{\nu'\lambda'}_{\nu\lambda})^4_\pm+2q_z^2[2\mathrm{k}_\parallel^2\pm(Q^{\nu'\lambda'}_{\nu\lambda})^2_\pm]} \times \Theta(E^{\eta}_{\nu\lambda}(\mathbf{k})-E^{\eta'}_{\nu'\lambda'}\pm\hbar\omega_{LO}+\Delta_{\lambda\lambda'}) \quad (8)$$

where Θ denotes the Heaviside step function, $m^\star$ is the electron effective mass, $\hbar\omega_{LO}$ is the longitudinal optical phonon energy, and ε_∞ and ε_S are the high frequency and static permittivity, respectively. The form factor is given by

$$\mathrm{F}^{\nu\lambda}_{\nu'\lambda'}(q_z)=\int_0^{3L} dz\,\Psi^\star_{\nu'\lambda'}(z)\Psi_{\nu\lambda}(z)e^{iq_zz} \quad (9)$$

3.2 Intervalley scattering

The phonon-assisted intervalley electron transitions can be modeled through an intervalley deformation potential [19], and the intervalley scattering rate can be written as

$$\frac{1}{\tau^{\nu'\lambda'\eta'}_{\nu\lambda\eta}(\mathbf{k}_\parallel)} = \frac{Z_{\eta'}D^2_{\eta\eta'}m^{\eta'\star}_{\nu'\lambda'}}{2\hbar\rho E_{\eta\eta'}}\left(N_{\eta\eta'}+\frac{1}{2}\mp\frac{1}{2}\right)I^{\nu'\lambda'\eta'}_{\nu\lambda\eta} \times \Theta(E^{\eta}_{\nu\lambda}(\mathbf{k})-E^{\eta'}_{\nu'\lambda'}\pm E_{\eta\eta'}+\Delta_{\lambda\lambda'}) \quad (10)$$

where η and η' denote the initial and the final valley index, respectively. $D_{\eta\eta'}$ is the intervalley deformation potential constant, ρ is the mass density, $E_{\eta\eta'}$ is the intervalley phonon energy, and $Z_{\eta'}$ denotes the degeneracy of the final valley. The overlap integral is determined by

$$I^{\nu'\lambda'\eta'}_{\nu\lambda\eta}=\int dz|\Psi^{\eta}_{\nu\lambda}(z)|^2|\Psi^{\eta'}_{\nu'\lambda'}(z)|^2 \quad (11)$$

3.3 ADP and ODP scattering

Based on the assumption that the perturbation Hamiltonian is proportional to the derivative of the atomic displacement, the electron scattering rate with the assistance of acoustic phonons can be written in the following form [20]

$$\frac{1}{\tau^{\nu'\lambda'}_{\nu\lambda}(\mathbf{k}_\parallel)} = \frac{E^2_{ac}m^\star_{\nu'\lambda'}k_BT}{\rho\hbar^3v_s^2}I^{\nu'\lambda'}_{\nu\lambda} \times \Theta(E_{\nu\lambda}(\mathbf{k}_\parallel)-E_{\nu'\lambda'}+\Delta_{\lambda\lambda'}) \quad (12)$$

where E_{ac} is the acoustic deformation potential, ρ is the density of the material, and v_s stands for the sound velocity. This equation is only valid for $\hbar\omega_q \ll k_BT$, i.e. when the thermal energy is much larger than the energy of the phonon involved in the transition, and in the elastic approximation limit $\hbar\omega_q \to 0$.

In contrast to the case of acoustic vibrations, the perturbation Hamiltonian for the optical modes is assumed to be proportional to the atomic displacement [21]. The scattering rate caused by optical phonons is given by

$$\frac{1}{\tau^{\nu'\lambda'}_{\nu\lambda}(\mathbf{k}_\parallel)} = \frac{E^2_{op}m^\star_{\nu'\lambda'}}{2\rho\hbar^2\omega_q}I^{\nu'\lambda'}_{\nu\lambda}\left(N_{op}+\frac{1}{2}\mp\frac{1}{2}\right) \times \Theta(E_{\nu\lambda}(\mathbf{k}_\parallel)-E_{\nu'\lambda'}\pm\hbar\omega_q+\Delta_{\lambda\lambda'}) \quad (13)$$

Due to the quite flat dispersion curve, the energy associated with optical phonons is assumed to be constant. Therefore, the phonon occupation number N_{op} is independent on the phonon wave vector. Formally, the scattering due to optical phonons with a deformation potential is treated in the same way as intervalley scattering.

4 Monte Carlo method

The ensemble Monte Carlo method is an efficient approach for solving the PME (2) and simulating electron transport in semiconductor devices in general [22]. It is based on calculating the motion of an ensemble of particles during a short time dt, where electrons are assumed to occupy a known energy state. Electrons can be subject to multiple scattering mechanisms such as electron-longitudinal optical (LO) phonon, acoustic and optical deformation potential, and intervalley scattering. These scattering mechanisms are considered to be instantaneous and satisfy transverse momentum conservation and total energy conservation.

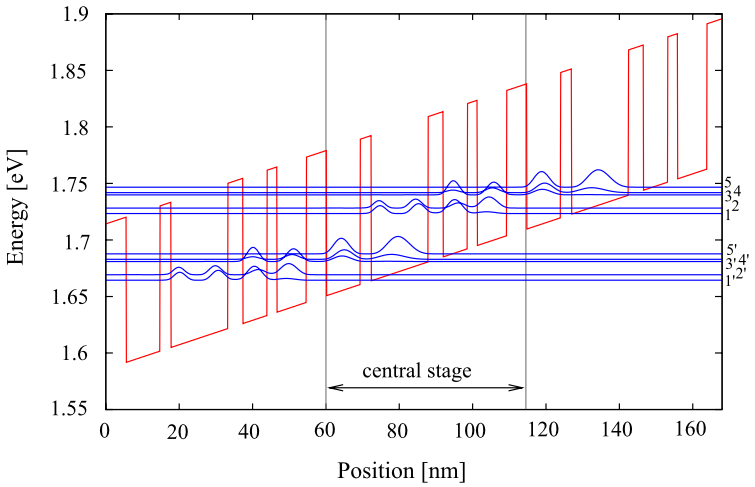

Fig. 2 Calculated conduction band diagram and squared wave functions for a $GaAs/Al_{0.15}Ga_{0.85}As$ QCL under an applied field of 10 kV/cm. The layer sequence of one cascade, in nanometers, is: 9.2,**3**,15.5,**4.1**,6.6,**2.7**,8,**5.5**, where normal scripts denote the wells and bold the barriers

Between two consecutive scattering events, which are chosen randomly under consideration of the probability of each scattering mechanism, the electron drifts force-free in the in-plane direction and remains in a given subband.

At the end of each free flight a scattering mechanism is selected, where each electron has its own probability of scattering depending on its energy and momentum. The selection of a scattering mechanism is made by means of the function Λ_n defined as

$$\Lambda_n(\mathbf{k}_\parallel) = \frac{1}{\Gamma}\sum_{i=1}^{n}\frac{1}{\tau_i(\mathbf{k}_\parallel)} \tag{14}$$

which are the successive summations of the scattering rates normalized with the total scattering rate Γ. By generating a random number r uniformly distributed in the range [0, 1], the n-th scattering mechanism is chosen according to [23]

$$\Lambda_{n-1}(\mathbf{k}_\parallel) < r \leq \Lambda_n(\mathbf{k}_\parallel) \tag{15}$$

The input for the Monte Carlo transport kernel is provided by a selfconsistent Schrödinger-Poisson solver.

Since QCL structures are considered unbound in the in-plane, the electron transport is determined by scattering between subbands.

In the simulation, electrons belonging to one stage are tracked. After obtaining the wave functions of the central stage and its neighboring stages, all relevant scattering parameters are determined. Current continuity is enforced by reinjecting every out-scattered electron into the central stage with an energy difference of $\Delta_{\lambda\lambda'} = \pm eFL$. The number of simulated electrons is chosen to provide for accurate results. In general, 5000 to 10,000 particles are sufficient for our semiclassical calculations. How many time steps are necessary to obtain a steady state solution depends mainly on the simulated structure itself. Usually, the required simulation time is between 5 and 30 ps. Since the Pauli exclusion principle is not considered, the concentrations of electrons should not be too high.

5 Simulation and results

Using the simulation scheme just described, we have calculated the steady state carrier distributions and the current-voltage characteristics of a QCL in the THz region. The structure considered consists of a combination GaAs wells and $Al_{0.15}Ga_{0.85}As$ barriers [24], and only the widest well is n-type doped with a low density of 1.8×10^{10} cm^{-2}.

Together with the squared envelope functions of the relevant bound states, the conduction band profile is plotted under an applied bias of 10 kV/cm in Fig. 2. The numerical values used for the relevant material parameters are listed in Table 1, where the difference in the electron affinity χ_e between the two materials determines the conduction band offset, and ϵ_S and ϵ_∞ denote the static and high frequency dielectric constants. For the given GaAs/AlGaAs system, these values are well established and can be looked up in [25] and [26].

The optical transitions occur between the subbands labeled 4, 3, and 2 which correspond to the upper and lower laser states. The lower laser state 2 is rapidly depopulated into the states 5′, 4′ or 3′ via LO-phonon emission. In order to maximize the speed of this process, the energy separation between these subbands should be close to the LO-phonon energy of the well material. Furthermore, the spatial overlap between the upper state 4 and the lower state 2 is kept as small as possible to increase the upper state lifetime. Figure 3 depicts the calculated LO-phonon rates $4 \rightarrow 4$ and $4 \rightarrow 3$. The energy of the initial states are given on the horizontal axis, and the zero energy reference value is taken at the bottom of subband 4.

Starting with a constant population initially assigned to each subband and using a constant time step of 5 fs we have

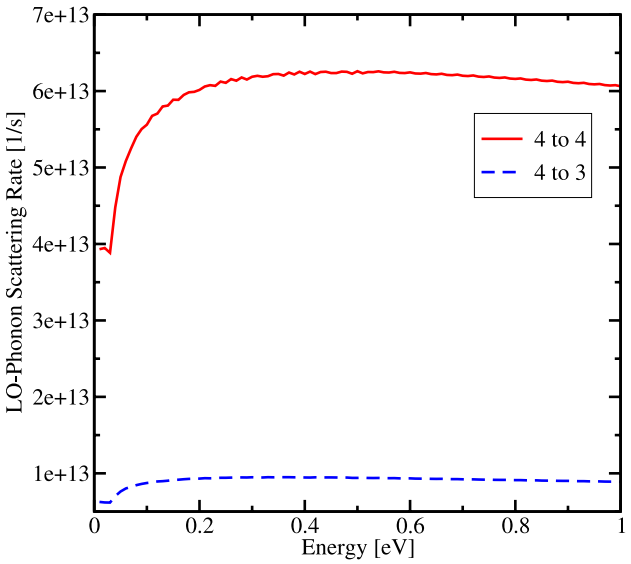

Fig. 3 Calculated LO-phonon scattering rates 4 → 4 and 4 → 3 at an applied bias of 10 kV/cm and an operating temperature of 70 K

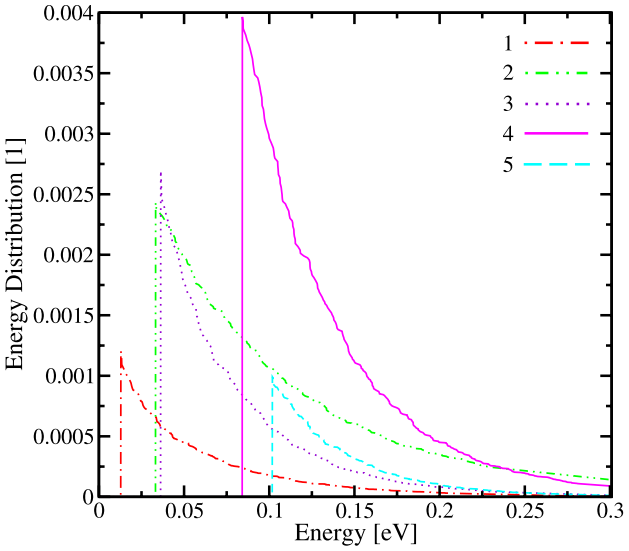

Fig. 5 Population of the individual subbands as a function of the kinetic energy

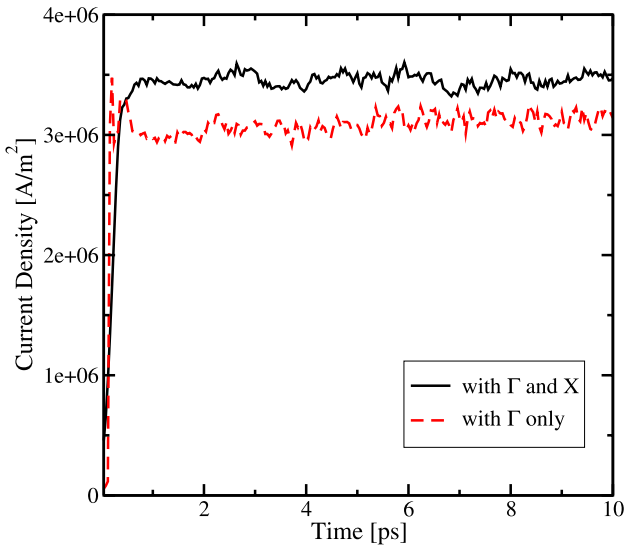

Fig. 4 Time evolution of the current density at an electric field of 10 kV/cm, with and without Γ-X intervalley scattering, illustrating the good convergence behavior

monitored 10,000 particles during 10 ps. Initially each subband has an equal number of particles, and subsequently the ensemble evolves until the simulation gets terminated. After each iteration step the distribution based statistics are updated. The numerical model for the QCL structure studied includes five subbands per stage and periodic boundary conditions are imposed.

Electron-LO phonon, acoustic and optical deformation potential, and intervalley scattering are included in the simulation with the relevant scattering rates computed at a temperature of 70 K and stored for each subband pair for a discrete number of initial electron energies.

Figure 4 shows the time evolution of the current density with and without Γ–X intervalley scattering at an electric field of 10 kV/cm. It can be seen that the inclusion of intervalley scattering increases the current density indicating that the Γ–X electron transfer plays a significant role as a mechanism for depopulation of the lower laser level. In Fig. 5, the obtained electron distributions of the individual subbands are depicted over the kinetic energy.

Additionally, the simulator has been used to simulate a GaAs/AlGaAs MIR QCL structure [27] and investigate the role of Γ–X intervalley scattering as a mechanism for the depopulation of the lower laser level, since a lot of interest arose for intervalley electron transfer in quantum well structures [28]. There, we proposed to modify the Al content and the width of the collection barrier of the given QCL design in order to increase the overlap between the upper X-state of the next stage and the lower Γ-state of the central one [29].

The current density obtained at an applied field of 10 kV/cm for the given THz design, which is illustrated in Fig. 4, suggests a similar influence of the intervalley electron transfer. Figure 6 displays the obtained current density with and without X valley transport, where the range of the applied bias is [10, 70] kV/cm and the chosen calculation step is 5 kV/cm. The results demonstrate that for this QCL structure the inclusion of Γ–X intervalley scattering leads to an increase in the current flow. Without Γ–X electron transfer the results are up to 10% lower. The output characteristics of the Monte Carlo simulation show that the effect of intervalley scattering processes is significant for the charge transport and not negligible in performance investigations.

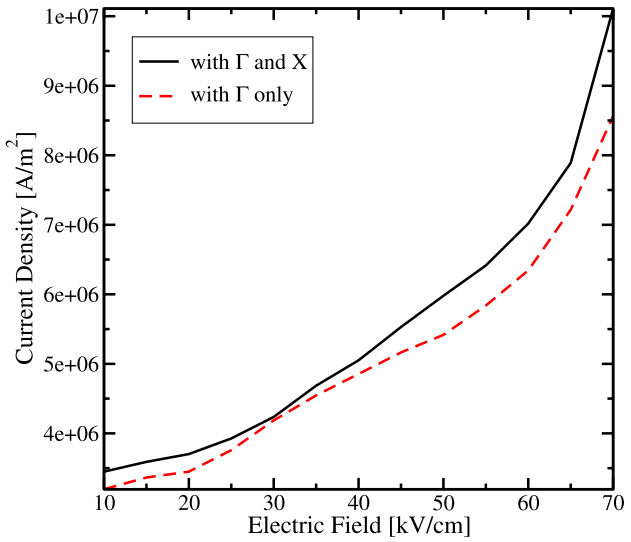

Fig. 6 Current density in dependence on the applied electric field with and without X valley transport

6 Conclusion

We have presented a rigorous Monte Carlo method based on a semiclassical transport description. The simulator has been used to simulate a GaAs based THz QCL structure. We have investigated the current density in dependence of the applied bias and the electron distribution functions of the individual subbands have been computed. Special focus was laid on the study of intervalley scattering effects on the carrier dynamics. In particular, the simulation results indicate that the Γ–X electron transfer plays a considerable role as a depopulation mechanism and highlights the importance of intervalley charge transport for QCL design considerations.

In general, it is demonstrated that the developed Monte Carlo simulator is an efficient approach for simulating stationary charge transport in quantum cascade structures governed by the PME.

Acknowledgements This work has been supported by the Austrian Science Fund, special research program IR-ON (F2509).

References

1. Esaki, L., Tsu, R.: Superlattice and negative differential conductivity in semiconductors. IBM J. Res. Dev. **14**, 61 (1970)
2. Kazarinov, R.F., Suris, R.A.: Possibility of the amplification of electromagnetic waves in a semiconductor with a superlattice. Sov. Phys. Semicond. **5**, 707 (1971)
3. Gmachl, C., Capasso, F., Sivco, D.L., Cho, A.Y.: Recent progress in quantum cascade lasers and applications. Rep. Prog. Phys. **64**, 1533 (2001)
4. Faist, J., Capasso, F., Sivco, D.L., Sirtori, C., Hutchinson, A.L., Cho, A.Y.: Quantum cascade laser. Science **264**, 553 (1994)
5. Lee, S.C., Wacker, A.: Nonequilibrium Green's function theory for transport and gain properties of quantum cascade structures. Phys. Rev. B **66**, 245314 (2002)
6. Iotti, R.C., Rossi, F.: Nature of charge transport in quantum-cascade lasers. Phys. Rev. Lett. **87**, 146603 (2001)
7. Matyas, A., Kubis, T., Lugli, P., Jirauschek, C.: Carrier transport in THz quantum cascade lasers: are Green's functions necessary? J. Phys. Conf. Ser. **193**, 012026 (2009)
8. Callebaut, H., Hu, Q.: Importance of coherence for electron transport in terahertz quantum cascade lasers. J. Appl. Phys. **98**, 104505 (2005)
9. Fischetti, M.V.: Theory of electron transport in small semiconductor devices using the Pauli master equation. J. Appl. Phys. **83**, 270 (1998)
10. Van Hove, L.: Quantum-mechanical perturbations giving rise to a statistical transport equation. Physica **XXI**, 517 (1955)
11. Zaccaria, R.P., Iotti, R.C., Rossi, F.: Monte Carlo simulation of hot-carrier phenomena in open quantum devices: a kinetic approach. Appl. Phys. Lett. **84**, 139 (2004)
12. Fischetti, M.V.: Master-equation approach to the study of electronic transport in small semiconductor devices. Phys. Rev. B **59**, 4901 (1999)
13. Weiss, U.: Quantum Dissipative Systems. World Scientific, Singapore (2008)
14. Iotti, R.C., Ciancio, E., Rossi, F.: Quantum transport theory for semiconductor nanostructures: a density-matrix formulation. Phys. Rev. B **72**, 125347 (2005)
15. Kittel, C.: Introduction to Solid State Physics. Wiley, New York (1996)
16. Iotti, R.C., Rossi, F.: Microscopic theory of semiconductor-based optoelectronic devices. Rep. Prog. Phys. **68**, 2533 (2005)
17. Frensley, W.R.: Boundary conditions for open quantum systems driven far from equilibrium. Rev. Mod. Phys. **62**, 745 (1990)
18. Rossi, F., Kuhn, T.: Theory of ultrafast phenomena in photoexcited semiconductors. Rev. Mod. Phys. **74**, 895 (2002)
19. Raichev, O.E.: Phonon-assisted Γ–X transfer in (001)-grown GaAs/AlAs superlattices. Phys. Rev. B **49**, 5448 (1994)
20. Bannov, N., Aristov, V., Mitin, V., Stroscio, M.A.: Electron relaxation times due to the deformation-potential interaction of electrons with confined acoustic phonons in a free-standing quantum well. Phys. Rev. B **51**, 9930 (1995)
21. Jacoboni, C., Reggiani, L.: The Monte Carlo method for the solution of charge transport in semiconductors with applications to covalent materials. Rev. Mod. Phys. **55**, 645 (1983)
22. Hockney, R.W., Eastwood, J.W.: Computer Simulation Using Particles. Taylor & Francis, London (1988)
23. Akarsu, M., Özbas, Ö.: Monte Carlo simulation for electron dynamics in semiconductor devices. Math. Comput. Appl. **10**, 19 (2005)
24. Benz, A., Fasching, G., Andrews, A.M., Martl, M., Unterrainer, K., Roch, T., Schrenk, W., Golka, S., Strasser, G.: Influence of doping on the performance of terahertz quantum-cascade lasers. Appl. Phys. Lett. **90**, 101107 (2007)
25. Adachi, S.: GaAs, AlAs, and $Al_xGa_{1-x}As$: material parameters for use in research and device applications. J. Appl. Phys. **58**, R1 (1985)
26. Madelung, O.: Semiconductors: Basic Data. Springer, Berlin (1996)
27. Pfluegl, C., Schrenk, W., Anders, S., Strasser, G., Becker, C., Sirtori, C., Bonetti, Y., Muller, A.: High-temperature performance of GaAs-based bound-to-continuum quantum-cascade lasers. Appl. Phys. Lett. **83**, 4698 (2003)
28. Rihani, S., Page, H., Beere, H.E., Ritchie, D.A., Pepper, M.: Design and simulation of a THz QCL based on Γ–X depopulation mechanism. Physica E **41**, 1240 (2009)
29. Milovanovic, G., Baumgartner, O., Kosina, H.: Design of a MIR QCL based on intervalley electron transfer: a Monte Carlo approach. In: Proceedings of the 10th International Conference on Mid-Infrared Optoelectronics: Materials and Devices (2010)